Suppressing Intermittent Subsynchronous Oscillation via Subsynchronous Modulation of Reactive Current

Jian Zhang, *Student Member, IEEE*, Xiangning Xiao, *Member, IEEE*, Peng Zhang, *Senior Member, IEEE*, Chao Luo, *Student Member, IEEE*, Yunsheng Wu, Jingjing Lu, *Student Member, IEEE*, and Lingyu Ren, *Student Member, IEEE*

***Abstract*—Recently, a new oscillation phenomenon—intermittent subsynchronous oscillation (ISSO)—has been observed in a large interconnected power grid. Rather than leading to oscillatory instability, ISSO causes cumulative fatigue damage and reduces the shaft life of the generator. The existing phase-compensation-based damping technologies are found to be limited in mitigating these types of oscillations. To mitigate ISSO, a subsynchronous modulation of reactive current (SMRC) approach is established and implemented in the voltage-source converters (VSCs) at the generator terminals. The contribution of SMRC to system damping has been analyzed in order to select control parameters for the VSC. The SMRC controller has been prototyped and extensively tested on a real-time closed-loop simulation platform equipped with a newly developed speed sensor module for precisely interfacing the real-time digital simulator with the rotating speed-acquisition board. Extensive experiments on the input and output characteristics of the VSC have been carried out to test and validate the damping current generating module. The effective damping areas are obtained from test observations to fine tune the parameters of the VSC controller for adapting to various system operating conditions, resulting in the common optimal damping region. Real-time simulations, onsite commissioning, and statistics have demonstrated the ability of the SMRC to mitigate ISSO and subsynchronous oscillation in power plants.**

***Index Terms*—Damping, fatigue accumulation, HVDC, intermittent subsynchronous oscillation (ISSO), real-time closed-loop test, subsynchronous modulation of reactive current, voltage-source converter (VSC).**

NOMENCLATURE

ISSO	Intermittent subsynchronous oscillation.
SMRC	Subsynchronous modulation of reactive current.
VSC	Voltage-source converter.
RTDS	Real-time digital simulator.
SSO	Subsynchronous oscillation.
HVDC	High-voltage dc transmission.
SDC	Supplementary damping controller.
SEDC	Supplementary excitation damping control.
TSR	Torsional stress relay.
SSDC	Subsynchronous damping controller.
SSR	Subsynchronous resonance.
FACTS	Flexible ac transmission system.
STATCOM	Static synchronous compensator.
PLL	Phase-locked loop.
GTAO	Gigabit transceiver analog output.
GTDI	Gigabit transceiver digital input.
FSC	Fixed series capacitor.
TCSC	Thyristor-controlled series capacitor.
FFT	Fast Fourier transform.
EDA	Effective damping area.
D_e	Electrical damping.
$\Delta\dot{T}_e$, $\Delta\dot{\omega}$	Incremental electromagnetic torque and rotating speed of complex number.
ξ	Angle difference between $\Delta\dot{T}_e$ and $\Delta\dot{\omega}$.
i_{qsub}	Critical-mode component passing through the damping current generating module.
I_q	Constant reactive current.
i_d, i_{dref}	Actual current and current reference in the d axis of VSC.
i_q, i_{qref}	Actual current and current reference in q axis of VSC.
$\Delta\omega_{\mathrm{crit}}$	Critical-mode component contained in $\Delta\omega$.
A, ω_m	Amplitude and angular frequency of $\Delta\omega_{\mathrm{crit}}$.
ΔU_{dc}	DC voltage variation.
k_p, k_i	PI gains in the outer loop of the SMRC controller.

Manuscript received November 15, 2014; revised February 17, 2015; accepted May 18, 2015. Date of publication June 17, 2015; date of current version September 21, 2015. This work was supported in part by the Fundamental Research Funds for the Central Universities under Grant 2015QN14 and in part by the National Science Foundation under Award CNS-1419076. Paper no. TPWRD-01382-2014.

J. Zhang and J. Lu are with the State Key Laboratory for Alternate Electrical Power System with Renewable Energy Sources, North China Electric Power University, Beijing 102206, China, and also with the Department of Electrical and Computer Engineering, University of Connecticut, Storrs, CT 06269 USA (e-mail: zj_369@163.com).

X. Xiao and C. Luo are with the State Key Laboratory for Alternate Electrical Power System with Renewable Energy Sources, North China Electric Power University, Beijing 102206, China.

P. Zhang and L. Ren are with the Department of Electrical and Computer Engineering, University of Connecticut, Storrs, CT 06269 USA (e-mail: peng@engr.uconn.edu).

Y. Wu is with Shanxi Electric Power Research Institute, Xian 710054, China.

Color versions of one or more of the figures in this paper are available online at http://ieeexplore.ieee.org.

Digital Object Identifier 10.1109/TPWRD.2015.2436063

k, γ	Gain and phase of the damping current generating module.
U_s, ω_0, θ_P	Amplitude, frequency, and initial phase of voltage at the connection point of VSC.
i_{ai}	Subsynchronous and supersynchronous currents output by the VSC in phase a.
i_{aiG}	Subsynchronous and supersynchronous currents injected into the generator in phase a.
α, θ	Proportion and phase deviation of the current flowing into the generator.
sub, *sup*	Subscript denoting subsynchronous and supersynchronous.
$i_{\alpha G}$, $i_{\beta G}$	Subsynchronous and supersynchronous currents injected into the generator under the $\alpha\beta$ coordinate system.
ψ_{d0}, ψ_{q0}	d- and q- component of the main flux linkage.
θ_0	Phase difference between the α-axis and d-axis.
q_s, Q_s	Instantaneous and constant reactive power output by the VSC.
ω_G	Generator speed obtained from the RTDS.

I. Introduction

SUBSYNCHRONOUS oscillation (SSO) is a detrimental phenomenon caused by the interaction between a generator and an external network consisting of series-compensated transmission lines [1]–[4] and/or HVDC [5]–[7]. A common form of SSO is undamped and continuous oscillations of the generator torque [8]. Divergent SSOs, however, seldom showed up in recent years because the strong coupling among interconnected subsystems tends to improve system damping [9]. On the other hand, as a new phenomenon, intermittent SSOs (ISSOs) have recently been discovered in an interconnected system with weak positive damping [10]. Although this new type of SSO is essentially convergent and does not result in immediate instability, it accelerates the shaft fatigue, significantly compromising the life of generators because of frequently intolerable oscillation amplitudes and may eventually lead to catastrophic consequences for generators. For instance, ISSOs have been recorded in several thermal power plants in the Northeast China Grid, resulting in serious generator fatigues [10].

The traditional way of alleviating SSO is to use the phase-compensation-based supplementary damping controller (SDC) where the damping of the entire system can be improved to a positive value. In [11], a combination of supplementary excitation damping control (SEDC) and torsional stress relay (TSR) was developed to solve the multimodal subsynchronous resonance (SSR) problem. However, the capacity of SEDC is generally limited by that of the excitation system. References [12]–[14] introduced subsynchronous damping control (SSDC) to damp multimodal SSOs in the ac/dc transmission grid by regulating the dc power of the HVDC line. Similarly, the performance of SSDC is limited by HVDC capacity [14], especially for ISSO problems existing in multi power plants. Besides, it has been observed in the real power system that SDCs, such as SEDC and SSDC, are unsuitable for ISSO mitigation [15].

The flexible ac transmission system (FACTS) is another kind of SSO mitigation method due to its flexible control ability, and may be designed with series or a shunt structure. Specially, shunt FACTS devices are more flexible to control and more convenient to connect with the system. The dynamic stabilizer is the first shunt FACTS which was proposed in [16] to mitigate SSO by regulating reactive power near the generator. Compared with the dynamic stabilizer, the voltage-source converter (VSC) based on full-controlled semiconductor devices has much faster response speed, stronger voltage independence, and damping ability [17], and smaller size with the same capacity. Besides, the gradually reduced cost will make the VSC more competitive. In [18], an SSR damping controller was implemented in STATCOM which was a kind of shunt VSCs and installed at the electrical center of a transmission line. However, the effectiveness of this approach for SSO and ISSO may be compromised because of its main function of reactive power compensation and long electrical distance between the controller and generator.

This paper introduces a new control method to effectively suppress ISSOs based on the understanding of the mechanism that triggers ISSOs. The main contributions of this paper include the following items: 1) A subsynchronous modulation of reactive current (SMRC) approach is introduced by combining gain and phase compensation, thereby effectively eliminating the intermittency in magnitudes; 2) the complex torque coefficient approach is established to quantify the damping provided by the SMRC; 3) a real-time closed-loop testbed with a new digital-physical interface between the RTDS and the generator speed acquisition board is designed to validate the effectiveness of the SMRC; and 4) a method to acquire effective damping areas (EDAs) is developed for optimizing the SMRC controller parameters and maximizing the ISSO mitigation effect.

This paper is organized as follows. Section II introduces the ISSO phenomenon and its characteristics. Section III presents the SMRC control strategy for mitigating ISSOs. Section IV provides technical details for setting up a real-time hardware-in-the-loop testbed for validating the SMRC. Experimental results and mitigation effects in the field are discussed in Section V, followed by Section VI that concludes this paper.

II. Intermittent Subsynchronous Oscillation

For a given generator, if the angle difference between the incremental electromagnetic torque and the incremental rotating speed is beyond $(-90^\circ, 90^\circ)$. At a certain torsional frequency, the system damping seen from this generator becomes negative and a growing oscillation, as illustrated in Fig. 1, will occur at this particular frequency [19]. This is the mechanism causing traditional SSO phenomena.

On the other hand, if the angle difference between the incremental electromagnetic torque and the incremental rotating speed is within the range of $(-90^\circ, 90^\circ)$, the system damping will be positive. However, if the system damping at a certain torsional frequency is weakly positive, the oscillations can still

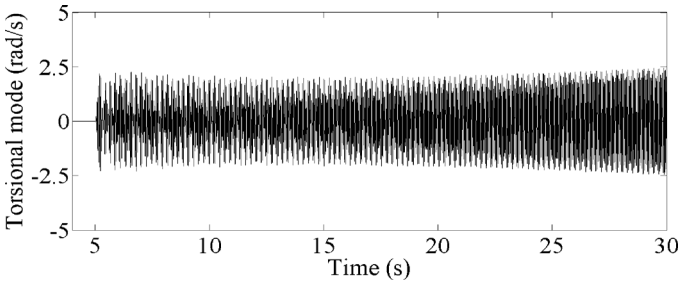

Fig. 1. Typical SSO based on the IEEE First Benchmark model.

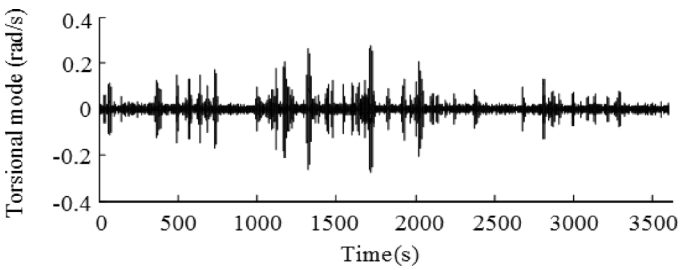

Fig. 2. Recorded ISSOs in a 2 × 600-MW power plant in the Northeast China Grid.

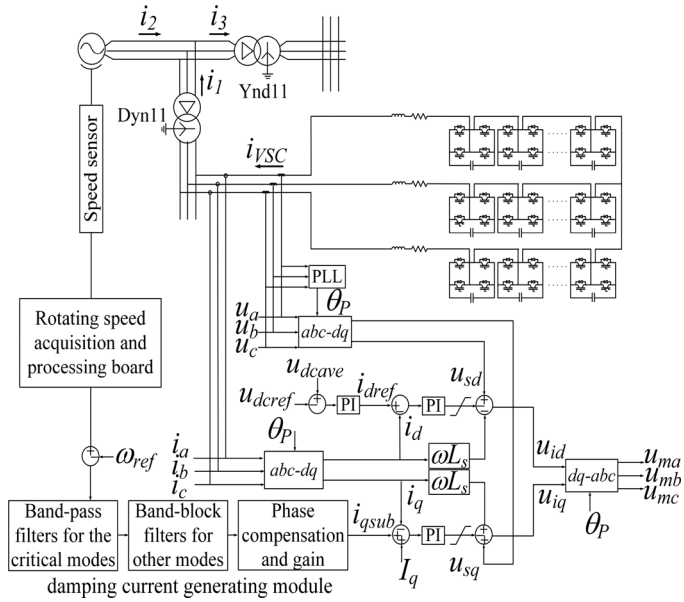

Fig. 3. Structure of the VSC and its control strategy.

be easily triggered, resulting in intermittent and convergent oscillations in the system, that is, ISSOs. An inherent characteristic of the ISSO is that the oscillation amplitude of the shaft can be intolerably high due to weak damping. Once triggered, the occurrence frequency of the ISSOs could be more than 100 times per day [15]. As a result, the generator will suffer severe cumulative fatigue damage. Fig. 2 shows this newly emerged phenomenon recorded in the field, where a power plant in the Northeast China Grid was impacted by ISSOs for about 5 to 20 times within an hour. Fortunately, a salient feature of the ISSO is that it takes a relatively long time for the amplitude to reach its peak due to positive damping and large inertia of the shaft, which makes it possible to mitigate ISSOs.

It is of critical importance to have further insight into the electrical damping D_e of the system. According to the complex torque coefficient approach [20], D_e can be expressed as

$$D_e = \frac{\left|\Delta \dot{T}_e\right|}{|\Delta \dot{\omega}|} \cos \xi \tag{1}$$

where ξ is the angle difference between the incremental electromagnetic torque $\Delta \dot{T}_e$ and the incremental rotating speed $\Delta \dot{\omega}$.

It can be seen from (1) that, for traditional SSOs caused by negative D_e, it is critical to change ξ in order to achieve a positive D_e. This explains why the phase-compensation-based approaches dominate the control strategies for mitigating divergent SSOs.

For ISSOs, however, D_e is normally positive by itself.[1] In order to reduce the oscillation amplitude of the ISSO, $\left|\Delta \dot{T}_e\right| / |\Delta \dot{\omega}|$ in (1) should be increased substantially to increase D_e. Certainly, it is also helpful to change ξ to further increase $\cos \xi$. Therefore, a controller that combines gain and phase compensation is desirable for mitigating ISSOs.

[1]Occasionally, D_e could be a small negative value. In this case, the mechanical damping in the system would make the overall damping weakly positive for an ISSO problem.

III. SMRC for Mitigating ISSO

The philosophy of the ISSO mitigation proposed in this paper is as follows. First, a local controller based on the VSC is adopted to produce controllable subsynchronous and supersynchronous currents which can be considered as a kind of modulation for the reactive current output by the VSC. Second, the currents are injected into the generator terminal in order to induce a rotating magnetic field in the rotor. Third, the electromagnetic torque at the subsynchronous frequency is produced by the rotating magnetic field. If the subsynchronous and supersynchronous currents are properly regulated, the electromagnetic torque will provide positive damping and eventually ISSOs will be mitigated. The advantages of this control strategy are threefold: 1) The controller is electrically close to the generator, meaning more damping current can be injected into the generator. Besides, local measurements such as the rotating speed are easily accessible for the local controller. 2) The controller is independent of the generator or HVDC capacity, meaning the control effect would not be compromised by the limitations of the existing equipment. 3) The reactive current regulation based on the VSC guarantees rapid responses. The following details the SMRC control design.

A. Control Strategy

The SMRC control strategy consists of *d*–*q* decoupling control, reactive current modulation control, and dc voltage control, as illustrated in Fig. 3.

The first is *d*–*q* decoupling control which separates the control of active and reactive currents.

The second is reactive current modulation control which takes the rotating speed of the generator as its input signal. The critical-mode component i_{qsub} is then extracted from the rotating speed deviation by the damping current generating module which consists of band-pass and band-block filters, phase compensation, and gain. i_{qsub} is used as the *q*–axis reactive current reference of the inner loop, together with the

constant reactive current I_q. In this way, the actual q–axis current produced by the VSC can respond to the oscillation component i_{qsub} in the rotating speed deviation in order to mitigate ISSOs.

The third is dc voltage control which takes the average of the capacitor voltages for H-bridge submodules as an input signal. The deviation of the average dc voltage from the reference voltage is then used as the d–axis active current reference of the inner loop. Through PI control, the actual d–axis current output from the VSC will be used to maintain the average dc voltage of the entire VSC. In addition, a balancing algorithm is also introduced to ensure the voltage balance among all of the VSC submodules [21].

B. Mechanism to Mitigate ISSOs

This subsection discusses how much damping can be generated by using the SMRC and how different factors could affect the performance of the SMRC.

The critical-mode component $\Delta\omega_{crit}$ contained in the rotating speed deviation is defined as

$$\Delta\omega_{\mathrm{crit}} = A\cos(\omega_m t) \tag{2}$$

where A and ω_m are the amplitude and angular frequency of the critical-mode component, respectively.

The amplitude and phase of the mode component will be changed after passing through the damping current generating module. Therefore, the q-axis reactive current reference can be expressed as

$$i_{\mathrm{qref}} = i_{\mathrm{qsub}} = kA\cos(\omega_m t + \gamma) \tag{3}$$

where k and γ reflect the amplification in the amplitude and phase shifting caused by the damping current generating module, respectively.

Note that, in industry practice, a VSC may also serve as a reactive power compensator equipped with a constant reactive power control which generally has no damping ability. Therefore, the constant reactive power control is ignored in the analysis of the damping mechanism.

Under ideal conditions, PI regulators work well and the actual q-axis current accurately tracks the reference value, then

$$i_q = i_{\mathrm{qref}} = kA\cos(\omega_m t + \gamma). \tag{4}$$

Similarly, the actual d-axis current may be expressed as

$$i_d = i_{\mathrm{dref}} = k_p\Delta U_{\mathrm{dc}} + k_i\int \Delta U_{\mathrm{dc}}. \tag{5}$$

Ideally, the dc voltage of the VSC is constant. Thus, ΔU_{dc} is zero and i_d is also zero [refer to (5)]. Then, the three-phase subsynchronous and supersynchronous currents output by the VSC can be calculated via the d—$qabc$ transformation

$$\begin{bmatrix} i_{ai} \\ i_{bi} \\ i_{ci} \end{bmatrix} = \begin{bmatrix} \cos(\omega_0 t+\theta_P) & -\sin(\omega_0 t+\theta_P) \\ \cos\left(\omega_0 t+\theta_P-\frac{2\pi}{3}\right) & -\sin\left(\omega_0 t+\theta_P-\frac{2\pi}{3}\right) \\ \cos\left(\omega_0 t+\theta_P+\frac{2\pi}{3}\right) & -\sin\left(\omega_0 t+\theta_P+\frac{2\pi}{3}\right) \end{bmatrix} \begin{bmatrix} i_d \\ i_q \end{bmatrix} \tag{6}$$

where ω_0 and θ_P are the fundamental frequency and initial phase of the voltage at the point where the VSC is connected. In practice, θ_P is acquired by a PLL.

From (6), the subsynchronous and supersynchronous currents in phase a of i_{VSC} (see Fig. 3) can be obtained as

$$\begin{aligned} i_{ai} &= -\sin(\omega_0 t+\theta_P)\cdot kA\cos(\omega_m t+\gamma) \\ &= -kA\sin\frac{((\omega_0-\omega_m)t+\theta_P-\gamma)}{2} \\ &\quad -kA\sin\frac{((\omega_0+\omega_m)t+\theta_P+\gamma)}{2}. \end{aligned} \tag{7}$$

According to Kirchhoff' s current law, part of i_{ai} flows into the grid, while the rest flows into the generator, as shown in Fig. 3. The latter can be expressed as

$$\begin{aligned} i_{aiG} &= \alpha_{\mathrm{sub}}kA\sin\frac{((\omega_0-\omega_m)t+\theta_P-\gamma-\frac{\pi}{6}+\theta_{\mathrm{sub}})}{2} \\ &\quad +\alpha_{\mathrm{sup}}kA\sin\frac{((\omega_0+\omega_m)t+\theta_P+\gamma-\frac{\pi}{6}+\theta_{\mathrm{sup}})}{2} \end{aligned} \tag{8}$$

where α is the proportion of the current flowing into the generator, θ denotes phase deviation, and subscripts sub and sup denote subsynchronous and supersynchronous components, respectively. Here, the phase deviation of $\pi/6$ is caused by the station transformer illustrated in Fig. 3.

The subsynchronous and supersynchronous currents under the $\alpha\beta$ coordinate system can be obtained by substituting (8) into the following transformation:

$$\begin{bmatrix} i_{\alpha G} \\ i_{\beta G} \end{bmatrix} = \frac{2}{3}\begin{bmatrix} 1 & -\frac{1}{2} & -\frac{1}{2} \\ 0 & \frac{\sqrt{3}}{2} & -\frac{\sqrt{3}}{2} \end{bmatrix} \begin{bmatrix} i_{aiG} \\ i_{biG} \\ i_{ciG} \end{bmatrix} \tag{9}$$

which gives

$$\begin{cases} i_{\alpha G} = \alpha_{\mathrm{sub}}kA\cos\frac{((\omega_0-\omega_m)t+\theta_P-\gamma-\frac{2\pi}{3}+\theta_{\mathrm{sub}})}{2} \\ \qquad +\alpha_{\mathrm{sup}}kA\cos\frac{((\omega_0+\omega_m)t+\theta_P+\gamma-\frac{2\pi}{3}+\theta_{\mathrm{sup}})}{2} \\ i_{\beta G} = \alpha_{\mathrm{sub}}kA\sin\frac{((\omega_0-\omega_m)t+\theta_P-\gamma-\frac{2\pi}{3}+\theta_{\mathrm{sub}})}{2} \\ \qquad +\alpha_{\mathrm{sup}}kA\sin\frac{((\omega_0+\omega_m)t+\theta_P+\gamma-\frac{2\pi}{3}+\theta_{\mathrm{sup}})}{2} \end{cases}. \tag{10}$$

According to [22], the incremental electromagnetic torque can be approximately expressed as

$$\begin{aligned} \Delta T_e = (\,-\psi_{q0} \quad \psi_{d0}\,) &\left\{\begin{bmatrix} \cos\theta_0 & \sin\theta_0 \\ -\sin\theta_0 & \cos\theta_0 \end{bmatrix}\begin{bmatrix} \Delta i_\alpha \\ \Delta i_\beta \end{bmatrix}\right. \\ &\left.+\left\{\begin{bmatrix} -\sin\theta_0 & \cos\theta_0 \\ -\cos\theta_0 & -\sin\theta_0 \end{bmatrix}\begin{bmatrix} i_{\alpha 0} \\ i_{\beta 0} \end{bmatrix}\Delta\theta\right\}\right. \end{aligned} \tag{11}$$

where ψ_{d0} and ψ_{q0} are the d- and q- components of the main flux linkage, respectively, and θ_0 is the phase difference between the α-axis and d-axis.

Substituting (10) into (11), the electrical damping coefficient provided by the VSC can be derived as

$$\begin{aligned} D_e &= k\psi_0\frac{\left[\begin{array}{l}\alpha_{\mathrm{sub}}\cos\left(\theta_s-\theta_P+\gamma-\theta_{\mathrm{sub}}+\frac{2\pi}{3}\right) \\ +\alpha_{\mathrm{sup}}\cos(\theta_s-\theta_P-\gamma-\theta_{\mathrm{sup}}+\frac{2\pi}{3})\end{array}\right]}{2} \\ &= \lambda k\psi_0\cos\frac{(\theta_s-\theta_P+\frac{2\pi}{3}-\rho)}{2} \end{aligned} \tag{12}$$

where

$$\begin{cases} \lambda = \sqrt{{\alpha_{\rm sub}}^2 + {\alpha_{\rm sup}}^2 + 2\alpha_{\rm sub}\alpha_{\rm sup}\cos(2\gamma - \theta_{\rm sub} + \theta_{\rm sup})} \\ \rho = \arctan\left(\frac{-\alpha_{\rm sub}\sin(\gamma-\theta_{\rm sub}) + \alpha_{\rm sup}\sin(\gamma+\theta_{\rm sup})}{\alpha_{\rm sub}\cos(\gamma-\theta_{\rm sub}) + \alpha_{\rm sup}\cos(\gamma+\theta_{\rm sup})}\right) \end{cases}. \tag{13}$$

It is indicated from (12) and (13) that the damping provided by the VSC mainly depends on the controller parameters k and γ, and the structure/condition of the external system reflected in $\alpha_{\rm sub}$, $\theta_{\rm sub}$, $\alpha_{\rm sup}$, and $\theta_{\rm sup}$. This means that k and γ should be properly chosen simultaneously in order to approach the maximum positive damping under most of the system operating conditions.

Now if the constant reactive power control functionality is taken into consideration in the VSC, the instantaneous reactive current is

$$i_q = i_{\rm qref} = kA\cos(\omega_m t + \gamma) + I_q \tag{14}$$

where I_q is the constant reactive current injected for reactive power compensation.

Rewrite the reactive current output in abc coordinates as follows:

$$\begin{cases} i_{ai} = -(kA\cos(\omega_m t + \gamma) + I_q)\sin(\omega_0 t + \theta_P) \\ i_{bi} = -(kA\cos(\omega_m t + \gamma) + I_q)\sin\left(\omega_0 t + \theta_P - \frac{2\pi}{3}\right) \\ i_{ci} = -(kA\cos(\omega_m t + \gamma) + I_q)\sin\left(\omega_0 t + \theta_P + \frac{2\pi}{3}\right) \end{cases}. \tag{15}$$

Equation (15) shows that the fundamental reactive current is modulated by the subsynchronous component at the frequency ω_m. By expanding (15), it can be seen that the reactive current actually contains fundamental, subsynchronous, and supersynchronous components.

The instantaneous reactive power output by the VSC is

$$q_s = u_d i_q - u_q i_d. \tag{16}$$

When the voltage at the generator terminal is in phase with the d-axis, according to (14) and (16), the reactive power can be expressed as

$$q_s = U_s kA\cos(\omega_m t + \gamma) + U_s I_q = Q(\omega_m t) + Q_s. \tag{17}$$

From the perspective of power, a subsynchronous component is superposed on the fundamental reactive power produced by the VSC. Equations (15) and (17) clearly show that ISSOs could be suppressed by regulating the reactive current/power.

IV. Real-Time Digital and Physical Closed-Loop Simulation Platform

A real-time digital and physical closed-loop simulation platform is built to validate the feasibility of the SMRC and to provide optimized controller parameters for the field commission, as shown in Fig. 4. It consists of the RTDS, the rotating speed acquisition, and processing boards, and the physical SMRC controller.

A. RTDS

Both the VSC and the test power system are modeled in the RTDS. In particular, the switching circuit of the VSC is modeled in the VSC Bridge Box provided by the RTDS to enable the simulation of power electronics with a time step between 1.4 and 2.5 μs. During the simulation, the VSC circuit is interfaced with the power system models by interface transformers, and with the real physical controller by the digital-to-analog or analog-to-digital card.

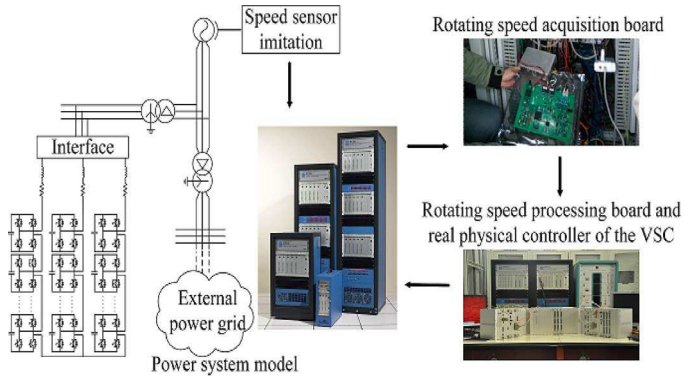

Fig. 4. Setup of the real-time digital and physical closed-loop ISSO mitigation test.

B. Rotating Speed Acquisition and Processing Boards

The rotating speed-acquisition board is used to receive data from the speed sensor installed on the generator shaft. The processing board then converts the speed data into the signals suited for the controller. Actually, the speed-acquisition board in the real power system is designed to take signals from the speed sensor which cannot be used in the simulation. In this paper, a method is designed to emulate the speed sensor in the RTDS so that the speed acquisition and processing boards can be integrated with the closed-loop simulation platform in real time. The procedures are as follows.

1) Identify the modulation method used in the speed sensor. Normally, frequency modulation is adopted in speed sensors. The output of the speed sensor is a sinusoidal signal with constant amplitude and varying frequency reflecting the generator speed.
2) Generate the frequency ω of the sensor data output by a linear equation, i.e.,

$$\omega = 60\omega_G \tag{18}$$

where ω_G is the generator speed obtained from the RTDS.
3) Evaluate the phase of sensor sinusoids by integrating ω, and then generate the output sinusoidal signal for the speed sensor.

The emulated sensor data are then sent to the rotating speed-acquisition and processing boards via the GTAO card of the RTDS.

The controller receives the generator speed from the rotating speed-processing board and receives the dc voltages of the submodules and the status signals from the RTDS. Then, it generates control signals and trigger pulses, and routes the signals back to the RTDS through the GTDI card of the RTDS.

V. Test Results

Extensive experiments are conducted on the power system where ISSOs were really detected. The effects of the SMRC in

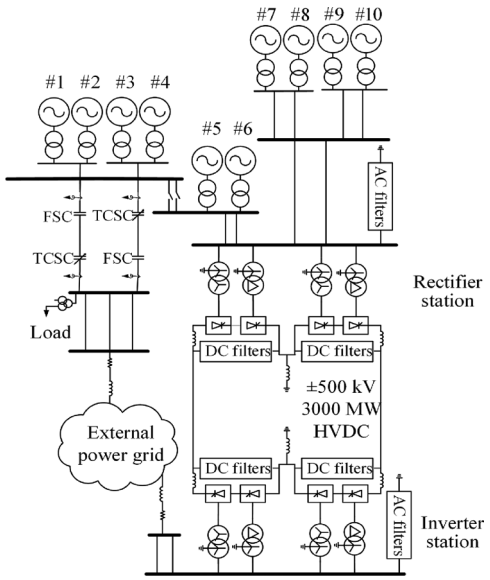

Fig. 5. One-line diagram of the bulk power system having an ISSO problem.

TABLE I
PARAMETERS OF THE VSC

Parameter	Value
Capacity	20 MVA
Rated voltage	10 kV
Cascaded number	6
Capacitor for sub-module	8400 μF
DC link voltage	2200 V
Carrier frequency	350 Hz
Connection reactance	2.2 mH
IEGT	4500 V/1500 A

mitigating ISSOs are tested in three aspects: 1) the VSC input and output characteristics; 2) the EDAs; and 3) the mitigation effect test under the disturbances.

The one-line diagram of the test system is shown in Fig. 5.

The power output from generators #1 to #4 is mainly delivered to the external grid through two identical 500-kV ac lines with 30% fixed series capacitor (FSC) compensation and 15% thyristor-controlled series capacitor (TCSC) compensation. The power from generators #5 to #10 is mainly transmitted to the external grid through a ±500-kV, 3000-MW bipolar HVDC. Generators 7 to 10 have more serious ISSO problems since most of their power is delivered by the HVDC, and the damping of every generator is weakened by the HVDC [10]. In the test below, the VSC based on the SMRC is connected to generator 7 to test its mitigation effect for ISSOs. The parameters of the VSC are listed in Table I.

The power flow through the HVDC and the operating states of the generators with an ISSO problem have a significant impact on the oscillation amplitude of the ISSO [15]. Therefore, various system operating conditions are selected for testing, of which three typical operating conditions are shown in Table II.

A. Input and Output Characteristics Test

A "frequency scanning" test based on time-domain simulation is introduced to verify the correctness of the SMRC controller design. The basic idea is: according to the input–output relationship of the VSC [refer to (7)], when an input signal at the frequency ω_m is injected, the VSC should produce three-phase currents with a subsynchronous component at $\omega_0 - \omega_m$ and a supersynchronous component at $\omega_0 + \omega_m$. And the phase difference between the two components is a constant 2γ. In order to mitigate ISSOs, the three-phase output currents should reach the peak when ω_m approaches the torsional frequency of the generator shaft.

In the test, the loop at the rotating speed-acquisition board (refer to Fig. 3) is first opened and a sinusoidal signal with controllable frequency is injected into the rotating speed-acquisition board and then the processing board. This test injection is to trigger the VSC to generate required subsynchronous and supersynchronous currents. Figs. 6–8 illustrate the amplitudes of the

TABLE II
OPERATING CONDITIONS

Condition	Power flow through HVDC	Generator #7	Generator #8
#1	3000 MW	Full output	Full output
#2	2000 MW	Full output	No output
#3	1000 MW	50% output	out of service

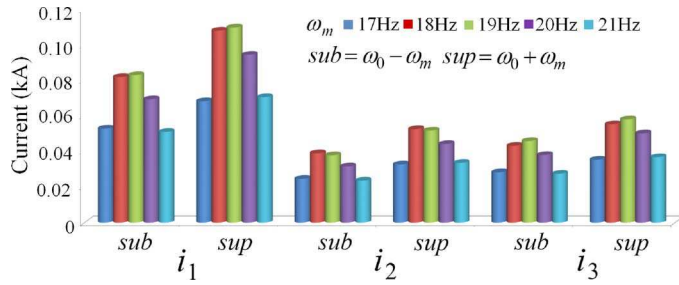

Fig. 6. Amplitude frequency characteristic of the subsynchronous and supersynchronous currents under condition #1.

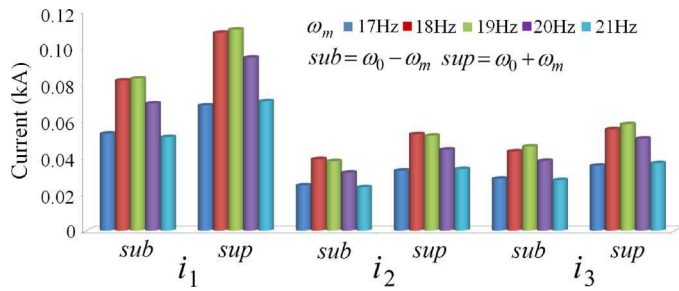

Fig. 7. Amplitude frequency characteristic of the subsynchronous and supersynchronous currents under condition #2.

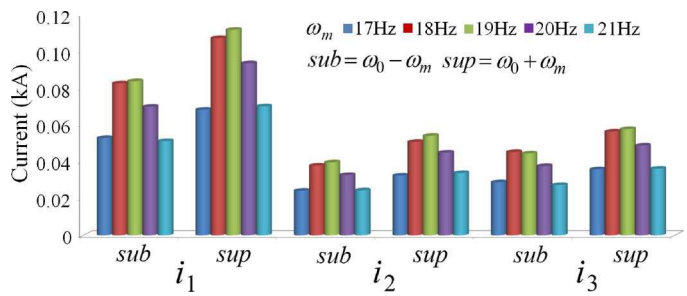

Fig. 8. Amplitude frequency characteristic of the subsynchronous and supersynchronous currents under condition #3.

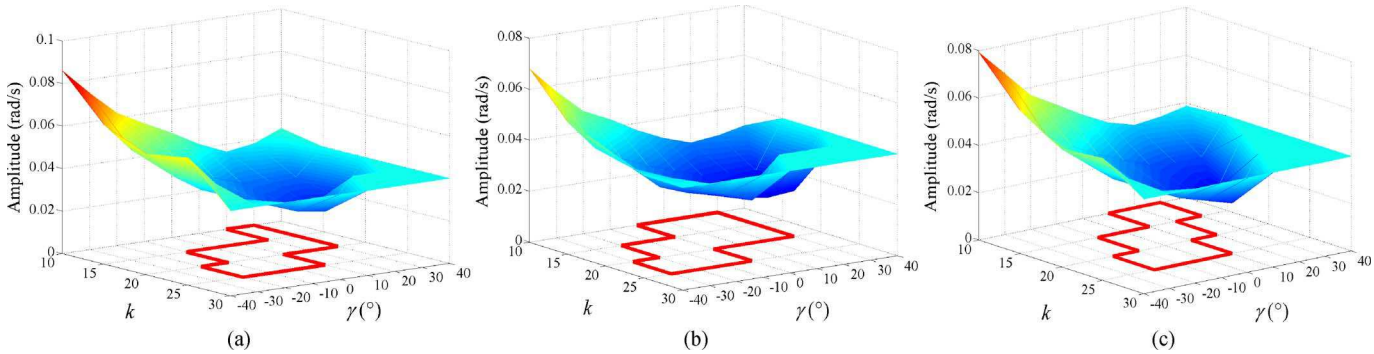

Fig. 9. Effective damping areas under the three system operating conditions: (a) Condition 1, (b) Condition 2, and (c) Condition 3.

TABLE III
PHASE CHARACTERISTIC OF THE SUBSYNCHRONOUS/ SUPERSYNCHRONOUSCURRENTS PRODUCED BY THE VSC

Amplitude of the test signal (p.u.)	2γ (°)		
	Condition #1	Condition #2	Condition #3
0.01	108.78	109.16	-250.71
0.02	108.90	108.80	-250.91
0.03	108.82	108.83	-251.02

current i_1 measured at the high side of the station transformer, the current i_2 flowing out of the generator, and the current i_3 flowing into the grid under the three operating conditions, respectively. The frequency varies between [17 Hz, 21 Hz], which includes the critical torsional frequency of the generator shaft (18.7 Hz). It can be seen from Figs. 6–8 that the largest amplitudes of the subsynchronous and supersynchronous currents appear near the torsional frequency. This proves that the damping current generating module is able to produce desirable control signals. An interesting finding is that the output characteristics of the VSC do not vary with the change of the operating conditions. This demonstrates the robustness of the SMRC control.

Further, the open-loop test is performed by injecting a sinusoidal signal at the critical torsional frequency (18.7 Hz) into the rotating speed-acquisition board and then the processing board. Changing the amplitude of the test signal from 0.01 to 0.03 p.u., the output current of the VSC is recorded. The phase differences between the subsynchronous component $\omega_0 - \omega_m$ and the supersynchronous component $\omega_0 + \omega_m$ are subsequently calculated through Fast Fourier transform (FFT). As can be seen from Table III, the phase difference between the subsynchronous and supersynchronous currents remains constant ($= 2\gamma$) despite the changes in the signal amplitudes and system operating conditions. This is consistent with the analysis in (7).

B. Identification of EDAs

According to (12) and (13), the damping capability provided by the VSC is partly determined by the system states that are uncertain and basically unadjustable. On the other hand, the damping capability is also determined by k and γ that are available for tuning. It is therefore desirable to identify a parametric space for k and γ, that is, the so-called EDA, such that, by setting k and γ in a common optimal damping region contained within the EDA, better SMRC performance can be ensured under most of the system operating conditions. The test is performed as follows.

The three system operating conditions are created in the RTDS. Without the VSC, the oscillation amplitudes of the ISSOs under the three operating conditions are, respectively, 0.3 rad/s, 0.22 rad/s, and 0.2 rad/s. With the VSC, for each test scenario, k and γ are changed in real time and the system responses to ISSO disturbances are recorded. All k and γ values that reduce the oscillation amplitudes to less than 0.1 rad/s (the cumulative fatigue threshold) are included in the EDAs as shown in Fig. 9.

As seen from Fig. 9, an EDA can be further divided into three regions:

1) Region 1: Weak Damping Control Region: This region describes the k and γ values that make the oscillation amplitude above 0.04 rad/s, which features smaller gain k and larger compensated phase γ. Normally, the region corresponds to a stable controller. However, the controller parameters in this region lead to poor damping performance because the large compensated phase is significantly displaced from the optimal compensated phase in region 3, and the gain is also insufficient.

2) Region 2: Sustained Oscillation Region: Large k and large γ will easily lead to a sustained oscillation of i_{VSC} when ISSO is detected, resulting in sustained mode oscillation with an amplitude of 0.04 rad/s as illustrated by the light blue region in Fig. 9. Large γ gives poor damping performance as mentioned before, while large k could make the SMRC run into the nonlinear region. What is worse, the region may correspond to an unstable region if no limits are considered in the VSC. In summary, this is a region to be avoided.

3) Region 3: Optimal Damping Region: Appropriately tuned k and γ can lead to optimal mitigation effects. In Fig. 9, the k-γ plane with the red boundary corresponds to the oscillation amplitudes below 0.04 rad/s. If found operating in any other region, the SMRC controller should be tuned in order to operate in this region.

According to the simulation results under various different operating conditions, a common optimal damping region can be finally determined with $k \in [15, 20]$ and $\gamma \in [-10°, 20°]$.

C. Time-Domain Validation

In this test, a disturbance is injected into the constant power controller of the HVDC rectifier station in order to stimulate ISSOs at the critical torsional mode corresponding to the frequency 18.7 Hz. If no countermeasure is taken, the ISSO amplitude would reach more than 0.2 rad/s, as illustrated in Fig. 10.

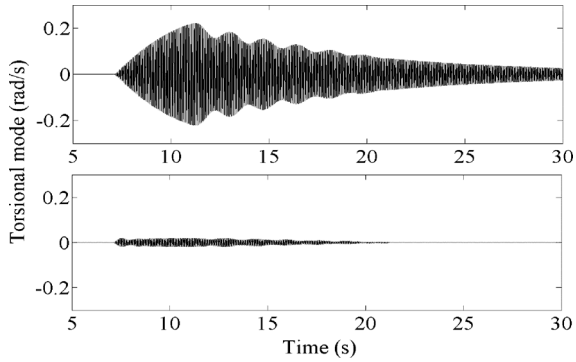

Fig. 10. Critical torsional-mode oscillation without and with the VSC under the small disturbance.

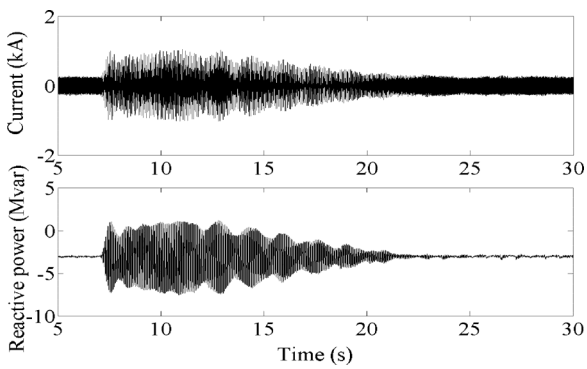

Fig. 11. Current and reactive power produced by the VSC under the small disturbance.

Once the VSC is switched in, the oscillation amplitude is reduced below 0.02 rad/s, which virtually eliminates the damaging cumulative fatigue in the shaft. Notice that in the steady state, the VSC is controlled to produce a small amount of reactive power (3 Mvar) as shown in Fig. 11, so that the dc voltage in the VSC could be better stabilized.

It also can be seen from Fig. 11 that the damping current modulates the fundamental reactive current produced by the VSC, while the damping power is superposed on the fundamental reactive power produced by the VSC. This is consistent with our analysis in (15) and (17).

In addition, a three-phase ground fault exerted on the commutation bus at the HVDC inverter station with the duration of 0.05 s is used to stimulate the large disturbance of the critical torsional mode. From Fig. 12, it can be seen that compared with the condition of no VSC, the rate of convergence of the mode oscillation can be distinctly improved with the VSC connected.

D. Field Statistics

The SMRC-based VSCs have been manufactured and successfully commissioned in the Northeast China Grid since March 2014. Two SMRC-based VSCs have been installed, respectively, in generators 7 and 8. The SMRC controller parameters, especially k and γ, were selected inside the common optimal damping region identified in this paper. The SMRC controllers completely mitigated the ISSO problems during the six-month operation. Figs. 13 and 14 show the torsional

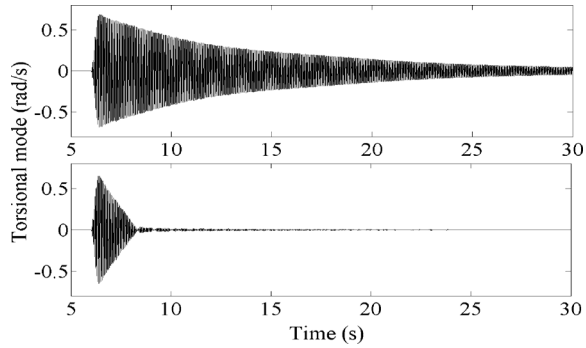

Fig. 12. Critical torsional-mode oscillation without and with the VSC under the large disturbance.

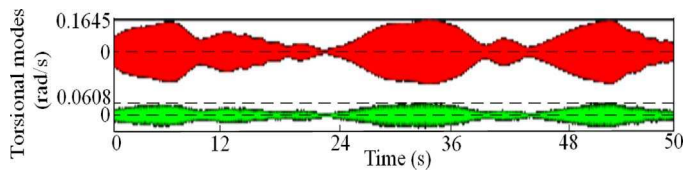

Fig. 13. Recorded torsional modes of Generator 7 without the VSC.

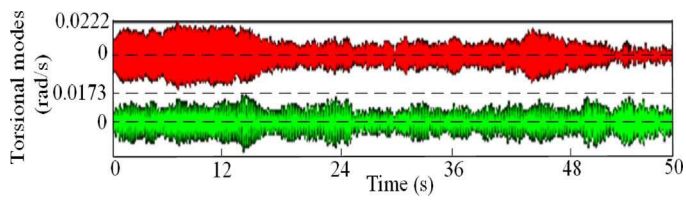

Fig. 14. Recorded torsional modes of Generator 7 with the VSC.

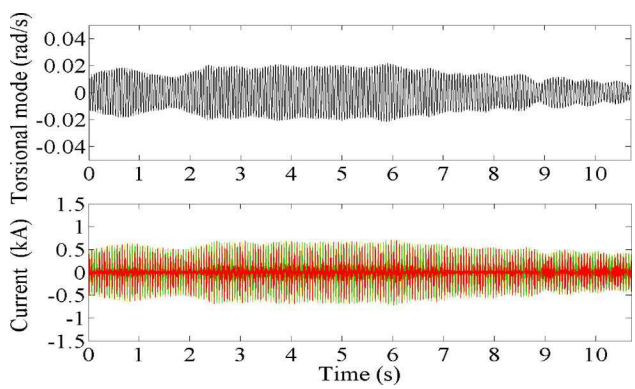

Fig. 15. Recorded critical torsional mode of Generator 7 and the corresponding three-phase output currents from the VSC.

modes of generator 7, respectively, with and without the VSC in two ISSO events under the same system operating condition. It can be seen that with the VSC, the oscillation amplitude of the vulnerable mode (in red) is significantly reduced from 0.1645 to 0.00222 rad/s. Fig. 15 shows another ISSO event for generator 7 and the corresponding three-phase currents output by the VSC.

Fig. 16 shows the statistics based on the operational data measured on April 10, 2014, including three test scenarios:

- Hours 1–9: The VSC on generator 7 was online while the VSC on generator 8 was out of service.

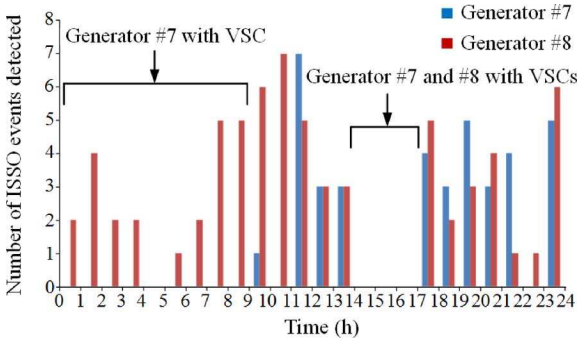

Fig. 16. Statistics of the ISSOs at generators 7 and 8 on 04/10/2014.

No ISSO events were detected at generator 7, meaning total mitigation was achieved by switching in the VSC on generator 7. Meanwhile, ISSO events were detected at generator 8 with a maximum of 5 times per hour (during hour 8 and hour 9). This striking statistics show the severity of the ISSO problem in this area and validate the benefits of the proposed SMRC method.

- Hours 15–17: Both VSCs were online. ISSO events were fully mitigated.
- Hours 10–14 and 18–24: Both VSCs were offline. ISSOs occurred several times each hour.

This shows that our approach has fully mitigated the long-standing ISSO issues existing in the area of generators 7 and 8. The field records, therefore, have validated the effectiveness of the SMRC-based VSC in this paper.

VI. Conclusion

The ISSO phenomenon emerging in recent years is introduced and analyzed in this paper. To effectively mitigate ISSOs, a new control strategy based on the SMRC control strategy is developed, which is implemented on the VSC at the generator terminal. A formula to quantify the damping effect of the SMRC is derived on the basis of the complex torque coefficient approach. The real-time closed-loop testbed is built to test and validate the SMRC control strategy. Extensive experiments are carried out to examine the input–output characteristics of the controller, to identify the common optimal damping region from the EDAs for controller parameters tuning, and to validate the effectiveness of the controller under small and large disturbances. The VSC based on the SMRC control strategy developed in this paper has been commissioned online and successfully mitigated the long-standing ISSO issues in a real power system.

Acknowledgment

The authors would like to thank anonymous reviewers for helpful discussions.

References

[1] D. Rai, S. O. Faried, G. Ramakrishna, and A. Edris, "An SSSC-based hybrid series compensation scheme capable of damping subsynchronous resonance," *IEEE Trans. Power Del.*, vol. 27, no. 2, pp. 531–540, Apr. 2012.

[2] Y. Cheng, M. Sahni, D. Muthumuni, and B. Badrzadeh, "Reactance scan crossover-based approach for investigating SSCI concerns for DFIG-Based wind turbines," *IEEE Trans. Power Del.*, vol. 28, no. 2, pp. 742–751, Apr. 2013.

[3] H. Xie, B. Li, C. Heyman, M. M. de Oliveira, and M. Monge, "Subsynchronous resonance characteristics in presence of doubly-fed induction generator and series compensation and mitigation of subsynchronous resonance by proper control of series capacitor," *IET Renew. Power Gen.*, vol. 8, no. 4, pp. 411–421, May 2014.

[4] C. E. Ugalde-Loo, J. B. Ekanayake, and N. Jenkins, "Subsynchronous resonance in a series-compensated Great Britain transmission network," *IET Gen., Transm. Distrib.*, vol. 7, no. 3, pp. 209–217, Mar. 2013.

[5] Chin Choo Yin, A. P. Agalgaonkar, K. M. Muttaqi, and S. Perera, "Subsynchronous torsional interaction behaviour of wind turbine-generator unit connected to an HVDC system," in *Proc. IECON*, 2010, pp. 996–1002.

[6] N. Rostamkolai, R. J. Piwko, E. V. Larsen, D. A. Fisher, M. A. Mobarak, and A. E. Poltras, "Subsynchronous torsional interactions with static VAR compensators-influence of HVDC," *IEEE Trans. Power Syst.*, vol. 6, no. 1, pp. 255–261, Feb. 1991.

[7] N. Prabhu and K. R. Padiyar, "Investigation of subsynchronous resonance with VSC-based HVDC transmission systems," *IEEE Trans. Power Del.*, vol. 24, no. 1, pp. 433–440, Jan. 2009.

[8] Chin Choo Yin, A. P. Agalgaonkar, K. M. Muttaqi, S. Perera, and M. Negnevitsky, "Analysis of subsynchronous torsional interaction of HVDC system integrated hydro units with small generator-to-turbine inertia ratios," *IEEE Trans. Power Syst.*, vol. 29, no. 3, pp. 1064–1076, May 2014.

[9] R. Zheng, X. Xiao, and J. Wang, "Subsynchronous oscillations study of non-parallel operating AC/DC system with series capacitor," in *Proc. China Int. Conf. Elect. Distrib.*, 2010, pp. 1–5.

[10] X. Xiao, J. Zhang, C. Guo, and L. Yang, "A new subsynchronous torsional interaction and its mitigation countermeasures," in *Proc. IEEE Energytech*, 2013, pp. 1–5.

[11] X. Xie, X. Guo, and Y. Han, "Mitigation of multimodal SSR using SEDC in the Shangdu series-compensated power system," *IEEE Trans. Power Syst.*, vol. 26, no. 1, pp. 384–391, Feb. 2011.

[12] Q. Y. Jiang, Y. J. Cao, and S. J. Cheng, "A genetic approach to design a HVDC supplementary subsynchronous damping controller," *IEEE Trans. Power Del.*, vol. 20, no. 2, pt. 1, pp. 1059–1064, Apr. 2005.

[13] D. J. Kim, H. K. Nam, and Y. H. Moon, "A practical approach to HVDC system control for damping subsynchronous oscillation using the noveleigenvalue analysis program," *IEEE Trans. Power Syst.*, vol. 22, no. 4, pp. 1926–1934, Nov. 2007.

[14] T. Rauhala and P. Jarventausta, "On feasibility of SSDC to improve the effect of HVDC on subsynchronous damping on several lower range torsional oscillation modes," in *Proc. IEEE Power Energy Soc. Gen. Meeting*, 2010, pp. 1–8.

[15] X. Xiao, J. Zhang, B. Gao, Y. Wu, C. Luo, C. Guo, and L. Yang, "Simulation and study on mitigation measures of frequent subsynchronous oscillation with low amplitude at multi power plants," *Sci China Tech Sci*, vol. 56, no. 6, pp. 1340–1353, Jun. 2013.

[16] D. G. Ramey, D. S. Kimmel, J. W. Dorney, and F. H. Kroening, "Dynamic stabilizer verification tests at the san juan station," *IEEE Trans. Power App. Syst.*, vol. PAS-100, no. 12, pp. 5011–5019, Dec. 1981.

[17] J. Zhang, X. Xiao, B. Gao, and C. Luo, "The comparative analysis of SVC and STATCOM on subsynchronous oscillation mitigation," *Adv. Mater. Res.*, vol. 756, pp. 245–249, Jun. 2013.

[18] K. Padiyar and N. Prabhu, "Design and performance evaluation of subsynchronous damping controller with STATCOM," *IEEE Trans. Power Del.*, vol. 21, no. 3, pp. 1398–1405, Jul. 2006.

[19] M. Bahrman, E. V. Larsen, R. J. Piwko, and H. S. Patel, "Experience with HVDC-turbine generator torsional interaction at Square Butte," *IEEE Trans. Power App. Syst.*, vol. PAS-99, no. 3, pp. 966–975, May 1980.

[20] A. Tabesh and R. Iravani, "On the application of the complex torque coefficients method to the analysis of torsional dynamics," *IEEE Trans. Energy Convers.*, vol. 20, no. 2, pp. 268–275, Jun. 2005.

[21] H. Akagi, S. Inoue, and T. Yoshii, "Control and performance of a transformerless cascade PWM STATCOM with star configuration," *IEEE Trans. Ind. Appl.*, vol. 43, no. 4, pp. 1041–1049, Jul./Aug. 2007.

[22] C. Yu, Z. Cai, Y. Ni, and J. Zhong, "Generalised eigenvalue and complex-torque-coefficient analysis for SSR study based on LDAE model," *Proc. Inst. Elect. Eng., Gen., Transm. Distrib.*, vol. 153, no. 1, pp. 25–34, Jan. 2006.

Jian Zhang (S'15) received the Ph.D. degree in electrical engineering from North China Electric Power University, Beijing, China, in 2014.

He was a Research Scholar with the University of Connecticut, Storrs, CT, USA, from 2013 to 2014. Currently, he is a Postdoctoral Researcher in control and computer engineering at North China Electric Power University. His research interests include power system stability, power system subsynchronous oscillation, power electronics, microgrid, and real-time simulation.

Xiangning Xiao (M'14) received the M.E. degree in electrical engineering from North China Electric Power University, Beijing, China, in 1981.

He was a Senior Research Scholar at the University of Bari, Bari, Italy, from 1991 to 1992. Currently, he is a Professor of electrical engineering at North China Electric Power University. His research interests include power electronics in the power grid with new energy resources, power quality and its improvement in power system, as well as power system subsynchronous oscillation.

Peng Zhang (M'07–SM'10) received the Ph.D. degree in electrical engineering from the University of British Columbia, Vancouver, BC, Canada.

He was a System Planning Engineer at BC Hydro and Power Authority, Vancouver, BC, Canada. He is an Assistant Professor of Electrical Engineering at the University of Connecticut, Storrs, CT, USA. His current research interests include power system resilience and reliability, microgrid, renewable energy systems, and wide-area measurement and control.

Dr. Zhang is a Registered Professional Engineer in British Columbia, Canada.

Chao Luo (S'13) received the B.E. degree in electrical engineering from Huazhong University of Science and Technology, Wuhan, China, in 2011 and is currently pursuing the Ph.D. degree in electrical engineering at North China Electric Power University.

His research interests include power system subsynchronous oscillation, power theory, power electronics, and real-time simulation.

Yunsheng Wu received the B.E. degree in electrical engineering from Xi'an Jiaotong University, Xi'an, China, in 1984.

Currently, he is a Senior Engineer at Shanxi Electric Power Research Institute, Xian. His research interests include power quality and power system subsynchronous oscillation.

Jingjing Lu (S'13) received the B.E. degree in electrical engineering from North China Electric Power University, Beijing, China, in 2010, where she is currently pursuing the Ph.D. degree in electrical engineering.

She was a Research Scholar at the University of Connecticut, Storrs, CT, USA, from 2013 to 2014. Her research interests include power quality and its improvement, power electronics, microgrid, as well as the unified power-quality conditioner.

Lingyu Ren (S'13) received the B.Sc. degree in electrical engineering from Shandong University, Jinan, China, the M.Sc. degree in electric power system and automation from the China Electric Power Research Institute, Beijing, China, and is currently pursuing the Ph.D. degree in electrical engineering at the University of Connecticut, Storrs, CT, USA.

Her research interests include power system resilience, microgrid, and distributed optimization.